Local structure around Mn and Co in $LaMn_{1-x}Co_xO_{3 \pm \delta}$: an EXAFS study



2009 J. Phys.: Condens. Matter 21 235405

(http://iopscience.iop.org/0953-8984/21/23/235405)

J. Phys.: Condens. Matter **21** (2009) 235405 (9pp) doi:10.1088/0953-8984/21/23/235405

# Local structure around Mn and Co in $LaMn_{1-x}Co_xO_{3\pm\delta}$: an EXAFS study

**Umesh A Palikundwar[1], V B Sapre[1], S V Moharil[1] and K R Priolkar[2]**

[1] Department of Physics, Rashtrasant Tukadoji Maharaj Nagpur University, Nagpur 440033, India
[2] Department of Physics, Goa University, Goa 403206, India

E-mail: uapali@yahoo.com

Received 3 November 2008, in final form 2 April 2009
Published 18 May 2009
Online at stacks.iop.org/JPhysCM/21/235405

**Abstract**

Detailed investigations of extended x-ray absorption fine structure (EXAFS) associated with the K-edges of Mn and Co have been carried out for $LaMn_{1-x}Co_xO_{3\pm\delta}$ ($0.3 \leqslant x \leqslant 1$) compounds. It is found that the local structure around Mn is different from that around Co. The distortion in $MnO_6$ octahedra decreases with the increasing Co content whereas $CoO_6$ octahedra are undistorted over the entire range of $x$. The Co–O bond length has been found to decrease with the increase in $x$. Based on the information about the first shell, the structural anomalies observed in these compounds have been discussed. Complementary information obtained from the XRD and EXAFS studies have been used to explain the behaviour of resistivity in these compounds.

(Some figures in this article are in colour only in the electronic version)

## 1. Introduction

Mixed valence manganites are the subject of intense scientific research due to their important properties such as antiferromagnetic (AM) to ferromagnetic (FM) transition followed by insulator to metal transition (MIT), charge ordering (CO) and orbital ordering (OO) [1–4]. Discoveries of giant magnetoresistance (GMR) and colossal magnetoresistance (CMR) [4] made them potential candidates for many technological applications such as magnetic sensors, magnetic recording, etc [5].

The rare earth manganites with perovskite structure of the formula $RMnO_3$ (where R is a trivalent rare earth ion) contain only $Mn^{3+}$ ions and are antiferromagnetic insulators [6]. The mixed valence state ($Mn^{3+}/Mn^{4+}$) is created either by partially substituting the rare earth ion by divalent ions like Ca, Ba, Sr, etc [7, 8], or by changing the stoichiometric oxygen content [9, 10]. The ferromagnetism and enhanced conductivity exhibited by these substituted or non-stoichiometric compounds are mainly due to the parallel alignment of spins by hopping of $e_g$ electrons through the $Mn^{3+}$–O–$Mn^{4+}$ double-exchange (DE) mechanism [1–4, 6–10].

Ferromagnetism is also observed in $RMnO_3$ wherein the Mn ion is partially substituted by other metal ions such as Co, Ni, Ga, etc [11–20]. The doping of Co at Mn site varies the number of electrons and hence changes the electronic configuration. Increasing Co content weakens the Mn–O–Mn interaction and the hopping range of $e_g$ electrons of undoped manganites. Mn–O bond distances and Mn–O–Mn angles also change due to the difference in the sizes of Mn and Co ions. In addition, due to the magnetic nature of Co ions, interactions such as Co–O–Co and Mn–O–Co are introduced [14]. All these interactions affect the physical properties of perovskite manganites/cobaltites, which are generally dependent on M–O–M bond angles and M–O bond distances (where M is either Mn or Co or both). The x-ray absorption fine structure (XAFS) studies would help in understanding the above effects. The XAFS can be divided broadly into two regions: (1) x-ray absorption near-edge structure (XANES) and (2) extended x-ray absorption fine structure (EXAFS). XANES provides the information about electronic structure and ionic state and EXAFS gives the local environment around the photo-absorbing ion [21].

Although extensive work has been carried out on $LaMn_{(1-x)}Co_xO_3$ compounds to understand their electrical and magnetic properties, only a few reports are available on their XAFS studies. Recently Sikora *et al* [22] have reported detailed investigations on XANES studies in these compounds.

 

**Table 1.** Oxygen off-stoichiometry ($\delta$) and unit cell parameters of $LaMn_{1-x}Co_xO_{3\pm\delta}$ ($0.3 \leqslant x \leqslant 1$) compounds. (Note: figures in the brackets next to each parameter are the uncertainties in the last digit.)

| | | | | Actual unit cell parameters | | | |
|---|---|---|---|---|---|---|---|
| $x$ | $\delta$ ($\pm 0.015$) | Goodness of fit $s$ | S.G. | $a$ (Å) | $b$ (Å) | $c$ (Å) | $v$ (Å$^3$) |
| 0.3 | −0.01 | 2.61 | *Pbnm* | 5.5286(6) | 5.4850(6) | 7.7715(8) | 235.6716 |
| 0.4 | −0.02 | 1.12 | *Pbnm* | 5.5150(4) | 5.4761(4) | 7.7673(4) | 234.5816 |
| 0.5 | −0.02 | 1.13 | *Pbnm* | 5.5211(7) | 5.4798(7) | 7.7644(1) | 234.9055 |
| 0.6 | −0.02 | 1.22 | $R\bar{3}C$ | 5.5055(1) | 5.5055(1) | 13.2244(1) | 347.1397 |
| 0.7 | −0.02 | 1.67 | $R\bar{3}C$ | 5.4857(1) | 5.4857(1) | 13.1839(1) | 343.6005 |
| 0.8 | −0.02 | 1.82 | $R\bar{3}C$ | 5.4750(1) | 5.4750(1) | 13.1598(1) | 341.6267 |
| 0.9 | −0.01 | 1.85 | $R\bar{3}C$ | 5.4548(7) | 5.4548(7) | 13.1192(9) | 338.0694 |
| 1 | 0.00 | 1.35 | $R\bar{3}C$ | 5.4442(1) | 5.4442(1) | 13.0975(2) | 336.1945 |

They have shown that Mn as well as Co gradually change their ionic states towards a higher oxidation state proportional to the Co content. The Mn and Co are respectively in mixed valence state as $Mn^{4+}/Mn^{3+}$ and $Co^{3+}/Co^{2+}$ throughout the entire range of $x$. Prochazka *et al* [23] have reported the local structure around Co for the first coordination shell through EXAFS studies. Similar to the findings of Sikora *et al* [22], they have also shown the increase in oxidation states of Co ions. The present work on EXAFS associated with the K-edges of Mn and Co in $LaMn_{1-x}Co_xO_{3\pm\delta}$, covering the composition range $x = 0.3$–1, has been undertaken to obtain information about the nature of the local environment around Mn and Co in the system. A detailed investigation on room temperature EXAFS for the first shell is reported. These compounds show orthorhombic to rhombohedral structural transition with Co substitution. At the local level it is observed that distortion in the $MnO_6$ octahedra decreases with increasing Co content while the $CoO_6$ octahedra remain undistorted over the entire composition range.

## 2. Experimental details

The compounds $LaMn_{1-x}Co_xO_{3\pm\delta}$ ($0.3 \leqslant x \leqslant 1$) were prepared from aqueous solutions of lanthanum nitrate, manganese acetate and cobalt acetate. The solution with an exact molar ratio was mechanically stirred for 1 h. The excess solvent was removed by heating the solution at 80 °C and a dry paste was obtained. This paste was then decomposed by heating at 500 °C in a furnace. The treatment enabled total dissociation of organic and nitrate materials. The resulting black powder was ground and heated at 1200 °C in air for 6 h. The compounds were then slowly cooled to room temperature.

The single-phase formation of the compounds was confirmed by the x-ray powder diffraction (XRD) method. The XRD data were collected using a PANalytical X'pert PRO diffractometer employing Cu K$\alpha$ radiation, with step size of 0.02° and scanning rate of 0.5° min$^{-1}$. The lattice parameters of the compounds were obtained by refining the XRD data by the Rietveld method using the software, FULLPROF [24]. The extent of oxygen non-stoichiometry ($\delta$) in the compounds was determined by iodometric titrations. Values of lattice parameters and $\delta$ are summarized in table 1. It is seen that all the compounds are stoichiometric within the limit of experimental accuracy. For $0.3 \leqslant x \leqslant 0.5$, the crystal structure is orthorhombic with *Pbnm* space symmetry while the compounds with $0.6 \leqslant x \leqslant 1$ are rhombohedral with $R\bar{3}C$ space symmetry. Rietveld refinement patterns for the boundary compounds $LaMn_{0.5}Co_{0.5}O_{3\pm\delta}$ and $LaMn_{0.4}Co_{0.6}O_{3\pm\delta}$ are shown in figures 1(a) and (b), respectively. The powder cell (PCW) programme [25] was used to visualize the crystal structure and also to calculate M–O–M bond angles and M–O bond lengths. The lattice parameters obtained from the Rietveld refinement were provided as input for the programme. The variation of average M–O–M bond angles and M–O bond lengths with $x$ is depicted in figure 1(c). Resistivity measurements were done using the standard four-probe method. The variation of resistivity with Co content ($x$) is shown in the inset of figure 6(b).

EXAFS at Mn and Co K-edges were recorded at room temperature in transmission mode on the EXAFS-1 beamline at the ELETTRA Synchrotron Source. Si(111) was used as the monochromator. For this, the powder of the sample was coated onto scotch-tape strips. The number of sample-coated strips was so adjusted that the absorption edge jump gave $\mu x \leqslant 1$. The incident and transmitted photon energies were simultaneously recorded using gas-ionization chambers as detectors. Measurements were carried out from 200 eV below the edge energy to 1000 eV above it with a 5 eV step in the pre-edge region and 2 eV step in the EXAFS region.

### 2.1. Data analysis

EXAFS fittings were carried out by the ifeffit 1.2.6 software package [26]. The energy calibration for the Mn/Co K-edge was done by assigning the energy value 6539/7709 eV to the first inflection point of the main edge in Mn/Co metal and aligning the spectra of all the compounds on the same scale. The threshold energy $E_0$ for all the compounds was taken as a maximum of the first derivative of the experimentally measured absorption coefficient $\mu(E)$. The EXAFS function $\chi(k)$ defined as $[\mu(k) - \mu_0(k)]/\mu_0(k)$ was obtained by subtracting a linear function obtained by fitting the pre-edge region (−200 to −50 eV with respect to the edge) from the entire raw spectra and the free atom background simulated by fitting a cubic spline function to the post-edge region (50–1000 eV beyond the edge). Here $k = (2m(E - E_0)/\hbar^2)^{1/2}$. The data in the $k$ range 3–13 Å$^{-1}$ were converted to $r$ space by Fourier-transforming (FT) $k^2$ weighted $\chi(k)$ through a

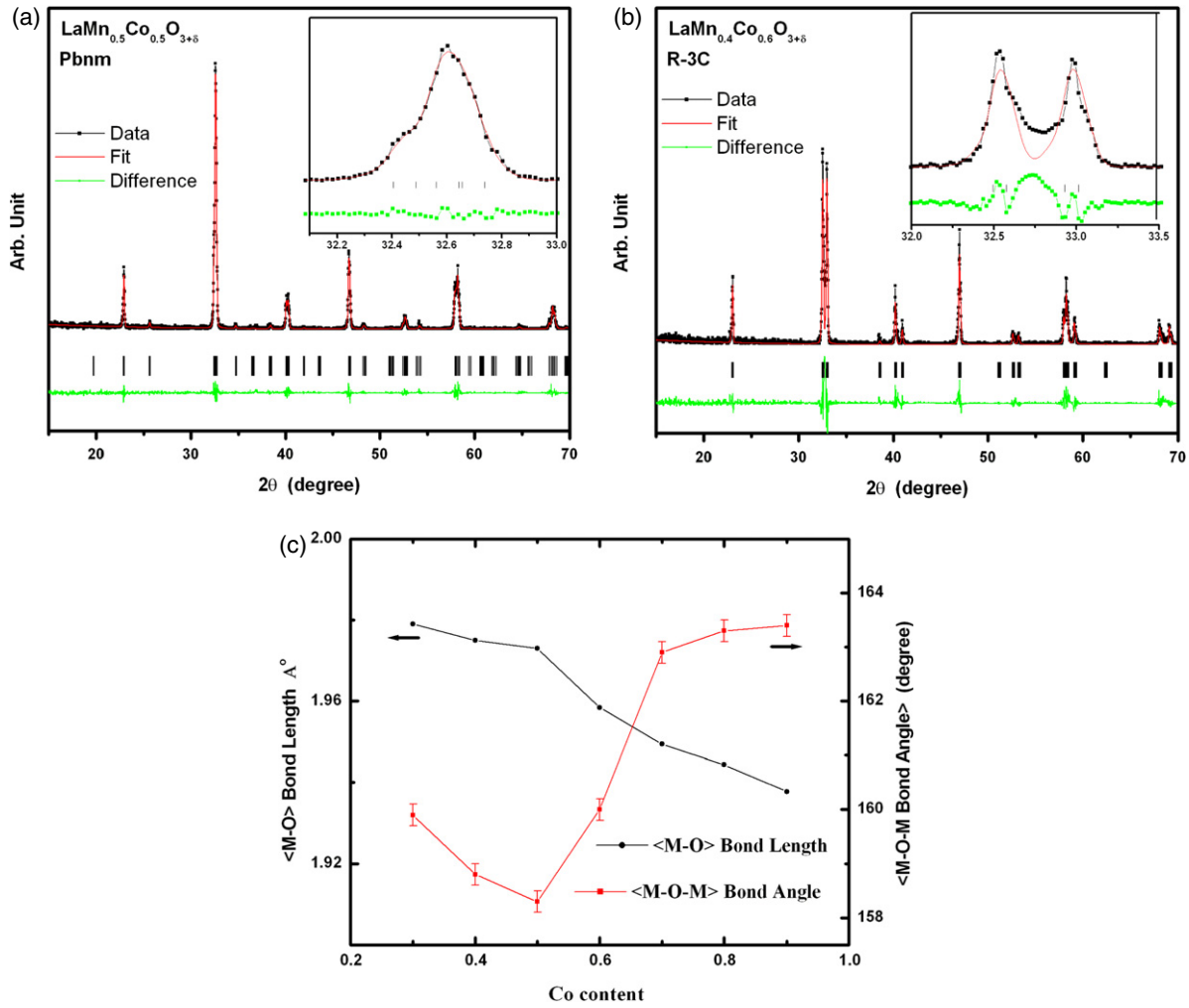


**Figure 1.** Rietveld refinement patterns of (a) $LaMn_{0.5}Co_{0.5}O_3$ and (b) $LaMn_{0.4}Co_{0.6}O_3$ compounds. (c) Variation of average M–O bond length and M–O–M bond angle with Co content.

Hanning window with the shape parameter d$k = 2$. The data were fitted with theoretical standards calculated using FEFF 6.01 [27] and ATOMS [28] using the structural parameters obtained from XRD analysis.

Based on the information obtained from the XRD data, we have tried different structural models in order to get the best information about the local structures in the compounds. The data were fitted using scattering paths obtained from the $Pbnm$ structure in the $4+2$ model while the scattering paths obtained from the $R\bar{3}C$ structure were used for fitting in the 6 model. During the fit, the number of nearest neighbours was initially kept fixed as per the model structure. The mean square relative displacement, $\sigma^2$, and change in bond distance, d$r$, were varied independently for each path. The change in the threshold energy, $\Delta E_0$, was first guessed for starting values of d$r$ and $\sigma^2$ as 0 Å and 0.003 Å$^2$, respectively. The amplitude reduction factor $S_0^2$ was kept fixed at 0.82 for all the compounds. The value of $S_0^2$ was decided from the best fit of the $LaCoO_3$ compound. A fit was considered to be good if the reliability parameter, given by the $R$ factor, was less than 0.02 [29]. Fitting was carried out for the first peak in Fourier filtered $k$ space. The $r$ range used for the first peak fittings was 0.9–1.9 Å. Slight variation was made in the higher limit, depending upon the spread of the peak for each compound. The number of independent points according to the Nyquist criterion was always greater than 6 for all the compounds. A Hanning window was also used for this back Fourier transformation. In the $Pbnm$ structure there are two short (1.91 and 1.96 Å) Mn–O bond lengths in the basal plane and one long (2.17 Å) along the apical axis. The two short bond lengths, being closer than the EXAFS resolution $\Delta R = \pi/2(k_{\max} - k_{\min}) \approx 0.16$ Å, were grouped into one correlation with a degeneracy of 4.

## 3. Results

Figures 2(a) and (b) show the $k^2$ weighted EXAFS spectra $\chi(k)$, of Mn and Co K-edges, respectively, for all the compounds. The spectra of Mn as well as Co EXAFS are highly structured. The Mn spectra show systematic variation in peak width, shape and amplitude with $x$, reflecting changes in the local structure around Mn. Co spectra also show the variation in shape, width and amplitude. The variation is large for the compounds with $x \geqslant 0.6$, indicating

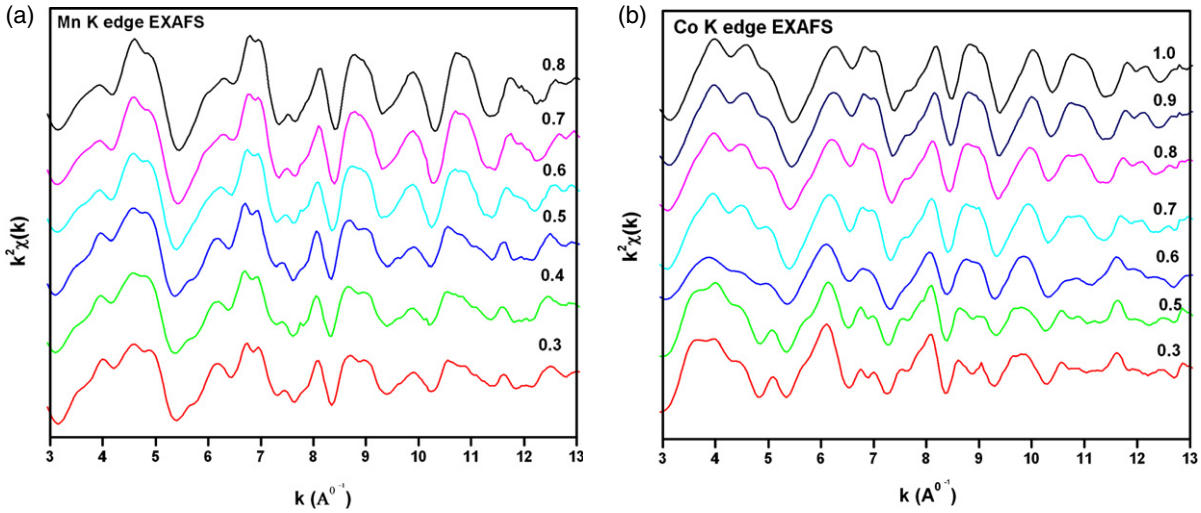


**Figure 2.** Variation of $k^2\chi(k)$, associated with (a) Mn K-edge and (b) Co K-edge, with $k$.

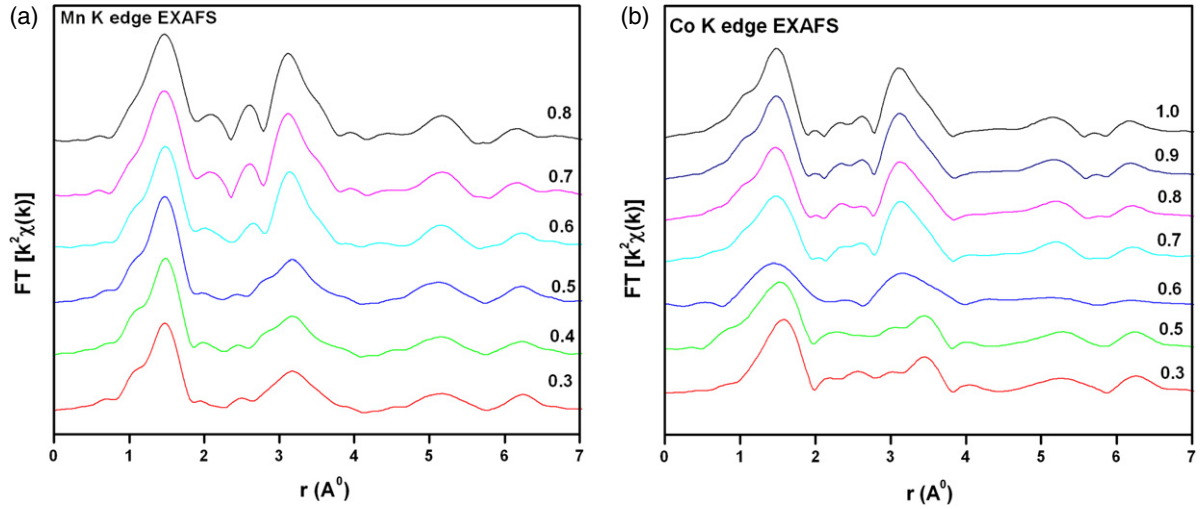


**Figure 3.** Variation of FT of $k^2\chi(k)$, associated with (a) Mn K-edge and (b) Co K-edge, with $r$.

a prominent change in local environment around Co for these compositions. Our XRD data also show orthorhombic ($Pbnm$) to rhombohedral ($R\bar{3}C$) phase transition for $x = 0.6$ composition. $k^2\chi(k)$ of Mn in the range 3–13 Å$^{-1}$ were Fourier-transformed and the magnitudes are presented in figure 3(a). The first strong peak around 1.5 Å in $r$ space is due to the contribution from the first coordination shell formed by the six oxygen atoms approximately located at a distance of 1.9 Å from the central Mn atom. The group of peaks in the range 2.2–4.2 Å is ascribed to the minor contribution from multiple scattering of the photoelectron within the first coordination shell, direct scattering from eight La atoms in the second shell, six Mn/Co atoms in higher shells and collinear multiple scattering due to Mn/Co–O–Mn/Co chains. Peaks at higher $r$ are ascribed to the atoms at higher shells. We observe that the amplitude of different peaks, associated with different shells, increases and becomes sharper with the increase in Co content, indicating reduction in the distortion of the first shell octahedron and increase in the symmetry at higher shells with doping. Figure 3(b) reveals FT of $k^2\chi(k)$ spectra for Co. The peaks similar to those in Mn are observed, suggesting the nearly similar environment around Co and Mn in the compounds. The amplitude of the peaks first decreases with increase in Co up to $x = 0.6$ and then increases with further increase in the Co content. This reflects increasing distortion of the octahedron or the one environment around Co up to $x = 0.6$ composition and the other for $x \geqslant 0.6$. The lowest amplitude for $x = 0.6$ indicates the distortion of the $CoO_6$ octahedron is largest for this composition.

Figures 4(a)–(c) show representative fits for the first shell of Mn K-edge EXAFS in Fourier-filtered $k$ space for $x = 0.3$, 0.5 and 0.8 compositions. It is evident from these figures that the structural model with two different Mn–O bond lengths, four short and two long (4 + 2 model), describes the experimental data well over the entire range of $k$ than that with six equal Mn–O bond lengths (6 model) for the lower $x$ ($x < 0.5$) compounds. This would imply that all the Mn–O bonds are not equal and that the $MnO_6$ octahedra are highly

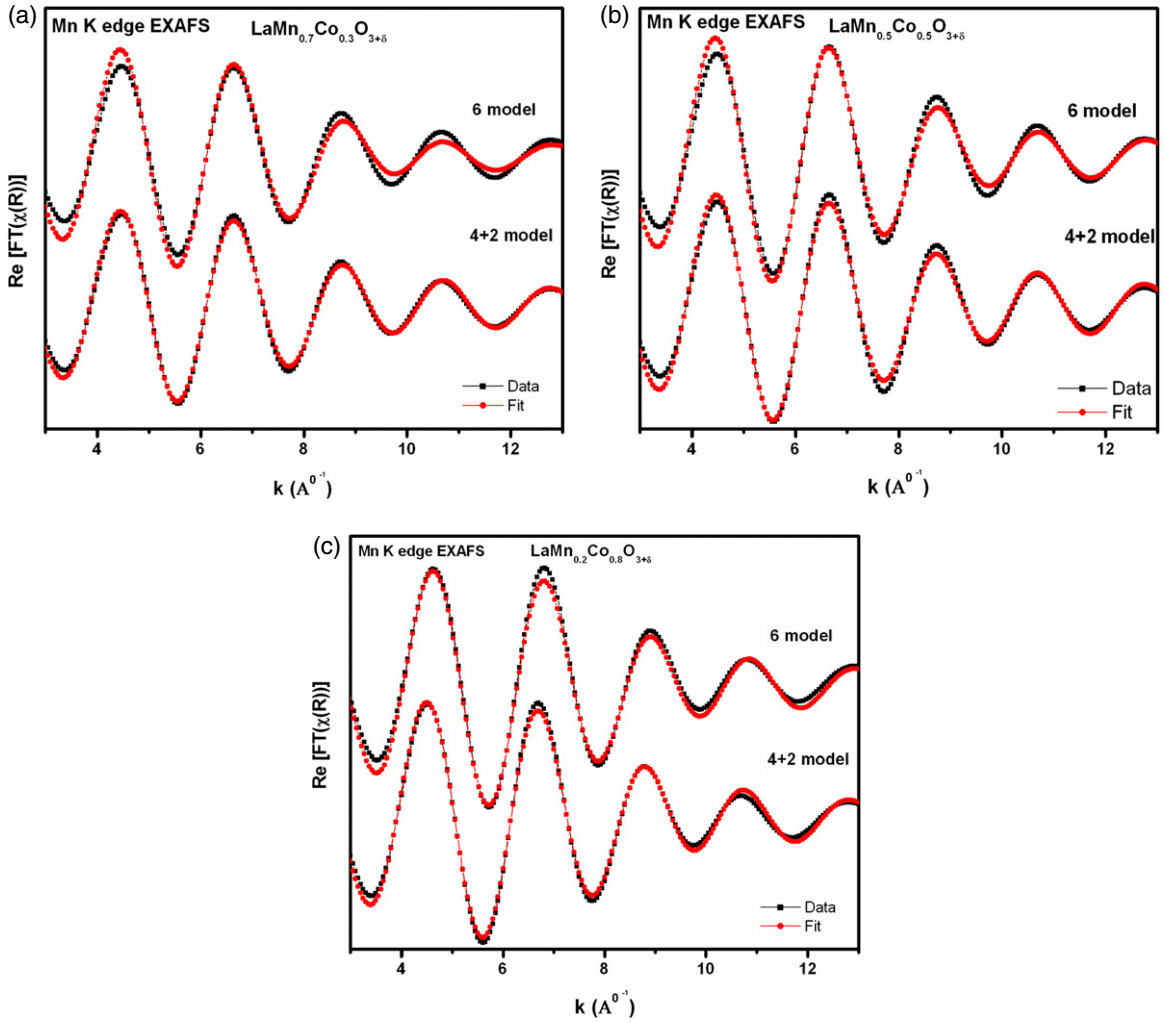


**Figure 4.** Fitting of real part of $k^2\chi(R)$ associated with Mn K-edge in Fourier-filtered $k$-space for (a) $LaMn_{0.7}Co_{0.3}O_3$, (b) $LaMn_{0.5}Co_{0.5}O_3$ and (c) $LaMn_{0.2}Co_{0.8}O_3$ compounds.

distorted in these compounds. The difference between the fits for the 4 + 2 and 6 models decreases with the increasing $x$ (figures 4(b) and (c)), which indicates that the distortion of the $MnO_6$ octahedra decreases with the increasing Co content. The complete descriptions of the paths included for the fittings and their resulting parameters for the first shell are summarized in table 2(a). The 4 + 2 model with two different Mn–O bond lengths gives one small and one large Debye–Waller (DW) factors for the compounds.

Similar types of fittings with one small and one large DW factors have also been shown by Shibata *et al* [30] and Subias *et al* [31] in their EXAFS studies of $La_{1-x}Sr_xMnO_3$ and $La_{1-x}Ca_xMnO_3$, respectively. The difference between long and short bond lengths is large for the $x < 0.5$ compounds, clearly indicating the existence of distorted $MnO_6$ octahedra. For the $x = 0.5$ compound the difference is close to the EXAFS resolution and it gives a very large DW factor (=0.017 Å$^2$) corresponding to a long bond length. In the 4 + 2 model, the number of nearest neighbours was kept fixed which suggests a homogeneous distribution of Mn ions and equal distortion in all $MnO_6$ octahedra. But now in the compounds, due to Co doping, a random distribution of Mn ions and/or alteration of $Mn^{4+}/Mn^{3+}$ ratio is possible [16, 22]. This may lead towards the change in the number of neighbours contributing to the short and long bond lengths. Therefore, such small and large DW factors respectively for short and long bond lengths (table 2(a)) may be due to the number of nearest neighbours contributing to the short bond length is more than 4 and that to the long bond length is less than 2. We have varied the number of nearest neighbours for long and short bond lengths, while keeping the total number at 6, contributing to the first peak to check this possibility for the $x = 0.5$ compound. The fit improves considerably when the number of neighbours of long and short bonds is 1.1 and 4.9, respectively, with corresponding DW factors of 0.010 and 0.0031 Å$^2$. The values of the bond lengths are found to be 1.91 and 1.96 Å, which are not resolvable. For the $x > 0.5$ compounds (not given in table 2(a)), the difference between bond lengths was found to be far below the EXAFS resolution limit. Looking at the closeness of the bond lengths and strong correlations between the parameters of the Mn–O subshells, similar to those observed in other doped manganites [30–34], we have tried

**Table 2.** Parameters obtained from Mn K-edge EXAFS first shell fittings with (a) 4 + 2 model and (b) 6C model for $LaMn_{1-x}Co_xO_{3\pm\delta}$ ($0.3 \leqslant x \leqslant 1$) compounds. (c) Parameters obtained from Co K-edge EXAFS first shell fittings with 6 model for $LaMn_{1-x}Co_xO_{3\pm\delta}$ ($0.3 \leqslant x \leqslant 1$) compounds. (Note: figures in the brackets next to each atom path are the degeneracy of atoms contributing to the path. Figures in the bracket next to each parameter are the uncertainties in the last digit. Uncertainties include systematic errors.)

(a)

| Co content | | 0.3 | 0.4 | 0.5 |
|---|---|---|---|---|
| $\Delta E_0$ (eV) | | −1.2(3) | −1.0(4) | −1.9(4) |
| *R*-factor | | 0.008 | 0.008 | 0.009 |
| O (4) | $r_1$ (Å) | 1.913(10) | 1.911(10) | 1.909(10) |
| | $\sigma_1^2$ (Å$^2$) | 0.0026(3) | 0.0022(3) | 0.0020(5) |
| O (2) | $r_2$ (Å) | 2.10(2) | 2.08(2) | 2.03(3) |
| | $\sigma_2^2$ (Å$^2$) | 0.0098(6) | 0.012(1) | 0.017(3) |

(b)

| Co content | | 0.3 | 0.4 | 0.5 | 0.6 | 0.7 | 0.8 |
|---|---|---|---|---|---|---|---|
| $\Delta E_0$ (eV) | | −3.5(11) | −3.2(12) | −4.1(11) | −3.2(11) | −2.5(15) | −2.8(12) |
| *R*-factor | | 0.008 | 0.009 | 0.011 | 0.009 | 0.009 | 0.011 |
| O (6) | $r_1$ (Å) | 1.911(10) | 1.908(10) | 1.901(10) | 1.902(10) | 1.900(12) | 1.901(12) |
| | $\sigma_1^2$ (Å$^2$) | 0.0089(10) | 0.0071(14) | 0.0055(10) | 0.0042(12) | 0.0036(18) | 0.0036(10) |
| | Cumulant (Å$^3$) | 0.000 09(2) | 0.000 06(2) | 0.000 05(3) | 0.000 008(6) | | |

(c)

| Co content | | 0.3 | 0.5 | 0.6 | 0.7 | 0.8 | 0.9 | 1.0 |
|---|---|---|---|---|---|---|---|---|
| $\Delta E_0$ (eV) | | −2.6(13) | −2.4(8) | −2.9(4) | −2.6(7) | −2.4(9) | −2.1(6) | −1.9(6) |
| *R* factor | | 0.007 | 0.009 | 0.012 | 0.005 | 0.009 | 0.006 | 0.004 |
| O (6) | $r_1$(Å) | 2.040(10) | 2.007(10) | 1.992(10) | 1.956(10) | 1.942(10) | 1.930(10) | 1.924(10) |
| | $\sigma_1^2$ (Å$^2$) | 0.0051(6) | 0.0069(9) | 0.0079(9) | 0.0068(6) | 0.0059(7) | 0.0046(5) | 0.0039(4) |

a cumulant expansion fitting with the six equal Mn–O bond lengths (6C model). The third cumulant, defined as $C_3 = \sigma^3$, was introduced in the fittings to account for the deviation of the atomic distribution in the first shell from the Gaussian symmetry. These fittings resulted in nearly equal Mn–O bond lengths (around 1.91 Å) for all the compounds (table 2(b)), as most of the spectral weight is due to the short bond lengths. The DW factor is large (≈0.009 Å$^2$) for the $x = 0.3$ compound and decreases with $x$. These are similar to the parameters resulting from the fittings with the 6 model. However, the *R* factor for these fittings was very high, 0.024, 0.021 and 0.019, respectively, for $x = 0.3$, 0.4 and 0.5 compounds, to be considered as a good fit [29]. The requirement of the cumulant in the fittings indicates that the distribution of the neighbours in the first coordination shell of Mn is non-Gaussian and that all the bond lengths are not equal, which is similar to the observation with the 4 + 2 model. The value of the cumulant decreases with the increase in Co content. For the compounds $x \geqslant 0.6$, the fit gives reasonable *R* factor values without use of the cumulant, i.e. similar to the 6 model.

Representative fits of Co K-edge EXAFS in Fourier-filtered $k$ space for $x = 0.3$, 0.5 and 0.8 are shown in figures 5(a)–(c). The 6 model describes the experimental data better than the 4 + 2 model, especially at higher $k$ values. The parameters, of the first shell, obtained from the fit with the 6 model, are described in table 2(c). Figure 6(a) shows the variation of DW factor of the first coordination shell obtained from the fits with the 6C model for Mn K-edge EXAFS. It can be seen that the DW factor ($\sigma_c^2$) decreases nearly linearly with Co. The value of the cumulant for $x = 0.3$ is $0.9 \times 10^{-4}$ Å$^3$ and decreases with $x$. For the $x = 0.6$ compound it becomes $0.8 \times 10^{-5}$ Å$^3$. The cumulant is not required in the fitting of the $x \geqslant 0.7$ compound. Figure 6(b) depicts the variation of DW factor ($\sigma^2$) of the first coordination shell obtained from the fits for Co K-edge EXAFS. $\sigma^2$ first increases in the range $0.3 \leqslant x \leqslant 0.6$ and then decreases for higher values of $x$ with a maximum at $x = 0.6$ composition.

For the Co K-edge EXAFS fittings, the 6 model with six equal Co–O bond lengths describes all the compounds with smaller *R* factor values than the 4 + 2 model. In this 6 model, six O atoms, equidistant from the central Co atom, form undistorted $CoO_6$ octahedra. The Co–O bond length obtained from the fit (figure 7) decreases linearly with the increase in $x$.

## 4. Discussion

The XRD studies have shown that the compounds are orthorhombic with *Pbnm* space symmetry for $0.3 \leqslant x \leqslant 0.5$ and rhombohedral with $R\bar{3}C$ space symmetry for $0.6 \leqslant x \leqslant 1$. In the orthorhombic compounds, the distortion in the $MnO_6$ as well as in $CoO_6$ octahedra is expected. However, EXAFS studies show that the $CoO_6$ octahedra are undistorted for all the compounds and that the distortion in the compounds is mainly due to the distorted $MnO_6$ octahedra. For the present case under study, the largest values of the DW factor and cumulant obtained from fitting with the 6C model (figure 6(a)) suggest the large distribution in Mn–O bond length and maximum distortion in $MnO_6$ octahedra for the $x = 0.3$ composition.

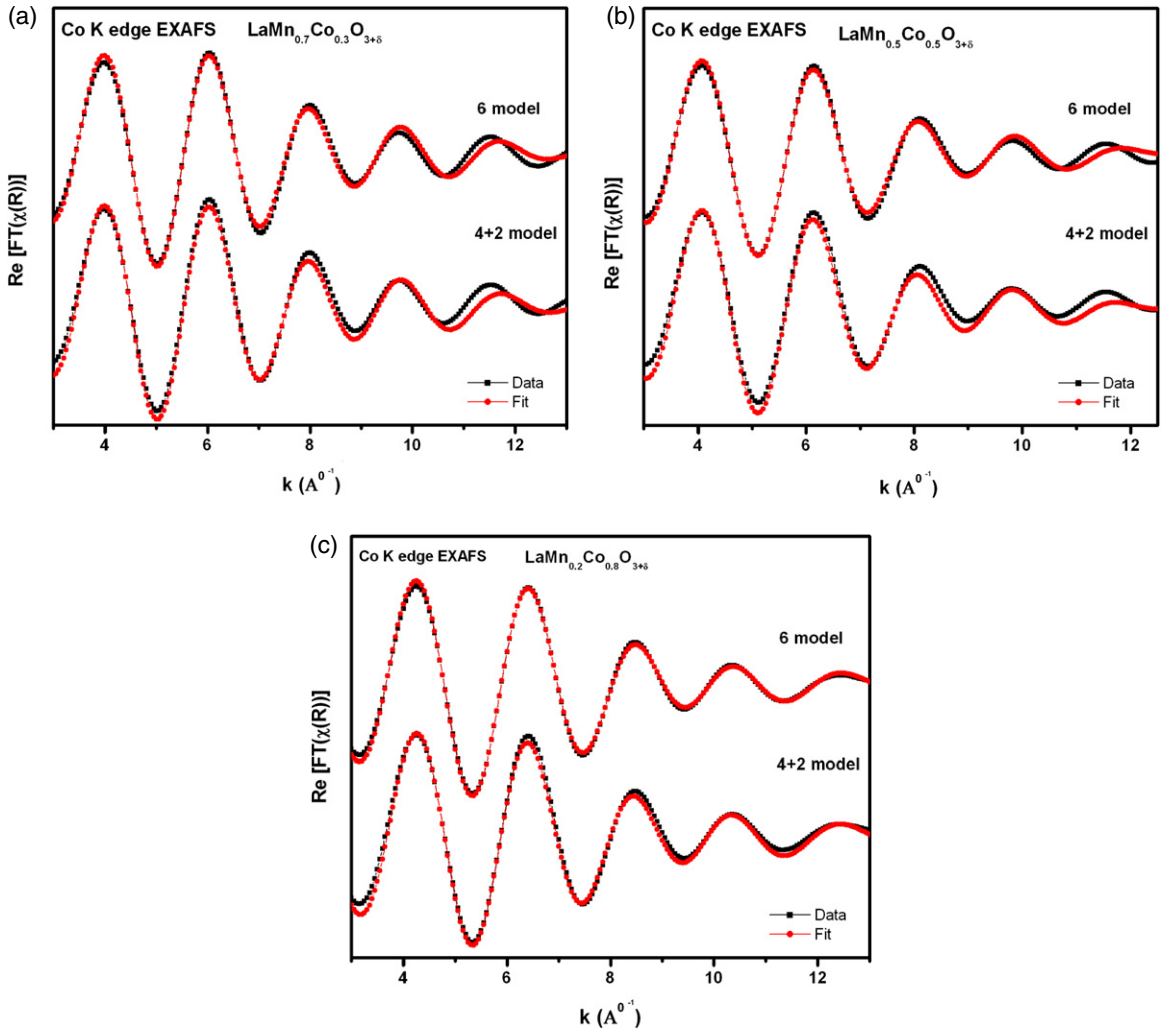


**Figure 5.** Fitting of real part of $k^2\chi(R)$ associated with Co K-edge in Fourier-filtered $k$ space for (a) $LaMn_{0.7}Co_{0.3}O_3$, (b) $LaMn_{0.5}Co_{0.5}O_3$ and (c) $LaMn_{0.2}Co_{0.8}O_3$ compounds.

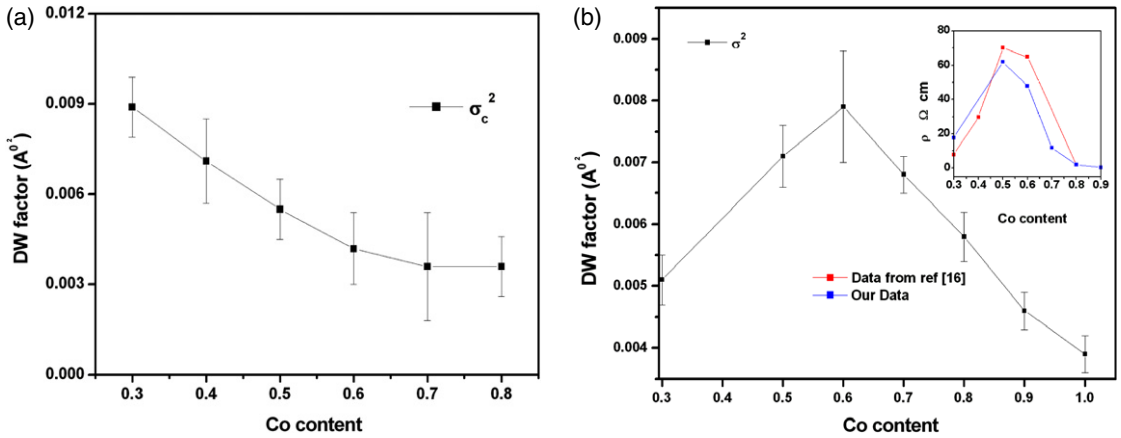


**Figure 6.** (a) Variation of Debye–Waller factor $\sigma_c^2$, obtained from Mn K-edge EXAFS fittings with 6C model, with Co Content. (b) Variation of Debye–Waller factor $\sigma^2$, obtained from Co K-edge EXAFS fittings with 6 model, with Co content. Inset: variation of room temperature resistivity with Co content.

The DW factor as well as the cumulant show a reduction with increasing $x$. This implies that the distortion in the $MnO_6$ octahedra reduces with increasing Co content. The distortion in the $MnO_6$ may be due to the presence of $Mn^{3+}$ ions. $Mn^{3+}$ is a strong Jahn–Teller (JT) type of ion and produces distortion in the octahedron at the local level to lift the degeneracy of

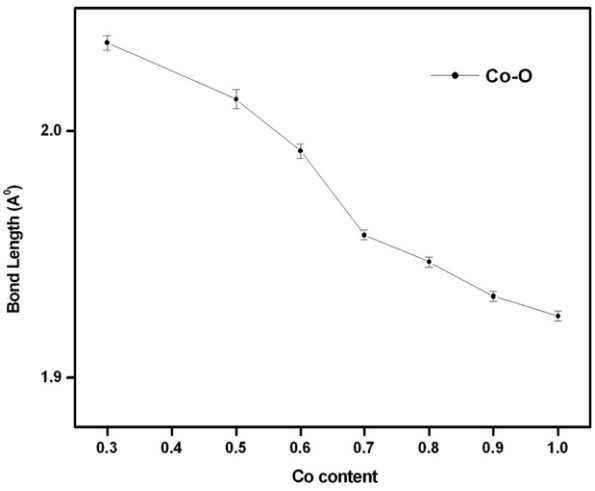


**Figure 7.** Variation of Co–O bond length, obtained from Co K-edge EXAFS fittings, with Co content.

$e_g$ orbitals. Our results indicate that the $Mn^{3+}$ ions in the compounds are decreasing and that the ratio $Mn^{4+}/Mn^{3+}$ in the compounds is increasing with the increase in $x$. For the $x \geqslant 0.7$ composition the 6C model gives a reasonable $R$ factor value without the use of the cumulant. As now a considerable number of Mn ions are replaced by Co ions and a large fraction of Mn is occupied by $Mn^{4+}$ ions, which are non-JT ions, the distortion in the $MnO_6$ octahedra reduces to a negligible value. The Co–O bond length obtained from the 6-model fittings (figure 7) shows contraction with the increase in $x$. This may be due to the reduction in the ionic size at the Co site, suggesting the increase in valence of Co with the increase in $x$. These results are well in agreement with the results obtained by Sikora *et al* [22] in their XANES studies of the compounds. They have also shown an increase in the valence state of Mn from +3 to +4 and that of Co from +2 to +3. The undistorted $CoO_6$ octahedron in orthorhombic compounds indicates the formation of different local structures around Co atoms substituted for Mn and the possibility of transition metal (TM) site ordering in the compounds. In Mn-rich compounds, XRD shows the average structure as orthorhombic while it is rhombohedral for Co-rich compounds. This may be due to the majority of distorted $MnO_6$ and undistorted $CoO_6$ octahedra in the respective regions. Several workers [11, 12, 16] have observed the structure as mixed orthorhombic and rhombohedral for the compounds near the boundary of these regions (i.e. for $x = 0.5$ and 0.6). By looking at the results of our EXAFS studies, one may find that the DW factor associated with the Co–O bond length changes the behaviour from the $x = 0.6$ composition. For this composition it is largest indicating the increased distortion in rhombohedral $CoO_6$ octahedra. Similarly the DW factor for Mn–O bond length is significantly larger for $x = 0.5$ and 0.6 compounds and the value of the cumulant reduces by a factor of 10 for the $x = 0.6$ compound. The small value of the cumulant for these compounds is also indicative of the small difference in the bond lengths forming the $MnO_6$ octahedra. This means that rhombohedral $CoO_6$ octahedra are highly distorted and $MnO_6$ octahedra are attaining the low distortion state in the boundary compounds. Therefore, slight variation in the stoichiometry of the compounds would result in orthorhombic, rhombohedral or mixed phase. Many researchers [35, 36] have also shown monoclinic $P2_1/n$ space symmetry for these boundary compounds and inferred the possibility of ordering of the TM site in the compounds. Our EXAFS studies also indicate the possibility of two distinct sites of TM ions, Co and Mn, and TM site ordering in the compounds. However, this is a possibility and has not been measured here. This can be verified by carrying out some site-specific studies.

The behaviour of resistivity in the compounds can be understood with the help of XRD studies and the variation of the DW factors. The insulating property is highly governed by the electron hopping probability from one Mn/Co site to the next Mn/Co site. If the bond length is more then there will be less overlapping of electronic wavefunctions and a smaller probability for the hopping of electrons. This will result in high resistivity. The average M–O bond length, as realized from our XRD (figure 1(c)) and EXAFS studies and also from the XANES studies by Sikora *et al* [22], decreases with the increase in Co content. This would imply that resistivity in the compounds should decrease as a result of the increase in the overlapping of electronic wavefunctions. However, the results regarding the resistivity obtained by us as well as Jonker [11] and Autret [16] (inset of figure 6(b)) are not as expected. Resistivity of the compounds increases first up to $x = 0.5$ then shows a reduction up to $x = 0.9$. The average M–O–M bond angle (figure 1(c)) decreases up to $x = 0.5$ and then increases with a further increase in $x$. DW factors give the measure of distortion in $MO_6$ octahedra and contain static and temperature components. We have carried out EXAFS measurements of all the compounds at the same temperature. Therefore, the temperature component of the distortion can be assumed to be the same in all the compounds and the variation of DW factors is mainly due to the static component. As discussed above, $MnO_6$ octahedra are highly distorted in $x \leqslant 0.5$ compounds due to additional JT distortion (unequal distribution of Mn–O bond lengths) of $Mn^{3+}$ ions and it is very difficult to isolate the contribution of distortion due to rotation/tilt of the octahedra in the DW factor. The DW factor corresponding to the Mn–O bond length decreases with $x$ as a result of the reduction in JT distortion. However, in $CoO_6$ octahedra, the contribution due to JT distortion is absent and the distortion due to rotation/tilt of $CoO_6$ octahedra is significantly reflected in the DW factor (figure 6(b)). The DW factor corresponding to the Co–O bond and the resistivity of the compounds (inset of figure 6(b)) varies in a similar fashion as that of M–O–M bond angle (figure 1(c)). Therefore, it is important to consider distortion due to the rotation of $MO_6$ octahedra along with M–O bond length while calculating the bandwidth of the overlapping of electronic wavefunctions as in the case of other manganite perovskites [37]. The electronic bandwidth ($W$) of the compounds in terms of bond length and rotation of $MO_6$ can be given as

$$W \propto \frac{\cos\omega}{d_{\mathrm{M-O}}^{3.5}}, \tag{4.1}$$

where $d_{M-O}$ is the average M–O bond length and $\omega$ is in the 'tilt' angle in the plane of the bond and is given by $\omega = \frac{1}{2}(\pi - \langle M{-}O{-}M\rangle)$ [37, 38]. Now for the compounds $x \leqslant 0.5$, the effect of decreasing average M–O bond length on $W$ is overridden by the decrease in the average M–O–M bond angle and increase in associated static distortion in the $MO_6$ octahedra. This results in a reduction of $W$ and increase in the resistivity. However, for the compounds $x > 0.5$, the bond length decreases whereas bond angle increases with $x$. Therefore, both these parameters contribute to an increase of the $W$. This is followed by the decrease in the resistivity. This clearly suggests that, along with the bond distances, distortion in the $MO_6$ octahedra also plays a crucial role in deciding the overlapping of electronic wavefunctions of two TM sites and the resistivity in the compounds.

## 5. Conclusions

Detailed analysis of EXAFS associated with the K-edges of Mn and Co clearly showed that the local structure of $MnO_6$ octahedra is distorted and the distortion decreases with the increase in Co content. In contrast, the $CoO_6$ octahedra are undistorted and have a single bond length for all six O atoms of the first coordination shell. The Debye–Waller factor is largest in $CoO_6$ octahedra for the composition $x = 0.6$, indicating the largest distortion in rhombohedral symmetry in the compound. The Co–O bond length and distortion in $MnO_6$ octahedra show a reduction with increasing Co content. This corresponds to the increase in oxidation state of both the TM ions. Complementary information obtained from the EXAFS and XRD studies could account for the observed variation in resistivity of the compounds.

## Acknowledgments

The authors are grateful to Dr Luca Olivi, Elettra, Synchrotron Source and Dr Vyankatesh Vyaghra, Department of Electronics, RTM Nagpur University, Nagpur for their help in EXAFS data collection. The work, carried out at Elettra, Synchrotron Source, Italy, was supported by the Department of Science and Technology (DST), Government of India and the Italian Government under the project Indo-Italian Programme of Cooperation (POC) in Science and Technology. The authors are also grateful to Dr Rajeev Rawat and UGC-DAE CSR, Indore for the support in resistivity measurements.

## References

[1] Ramirez A P 1997 *J. Phys.: Condens. Matter* **9** 8171
[2] Von Helmolt R, Wecker J, Holzapfel B, Schulz L and Sammer K 1993 *Phys. Rev. Lett.* **71** 2331
[3] Coey J M D, Viret M and von Molnar S 1999 *Adv. Phys.* **48** 167
[4] Tokunaga M, Miura N, Tomioka Y and Tokura Y 1998 *Phys. Rev.* B **57** 5259
[5] Day C 2007 *Phys. Today* **60** (December) 12
[6] Wollan E O and Koehler W C 1955 *Phys. Rev.* **100** 545
[7] Nam D N H, Phue N X, Bau L V, Khiem N V and Sau L H 2002 arXiv:cond-matt/020780 v1
[8] Li X, Fan X J, Ji G, Wu W B, Wong K H, Choy C L and Ku H C 1999 *J. Appl. Phys.* **85** 1663
[9] Ritter C, Ibarra M R, De Terasa J M, Algarabel P A, Marquina C, Blasco J, Garcia J, Oseroff S and Cheong S 1997 *Phys. Rev.* B **56** 8902
[10] Dezanneau G, Audier M, Vincent H, Meneghini C and Djurado E 2004 *Phys. Rev.* B **69** 014414
[11] Jonker G H 1966 *J. Appl. Phys.* **37** 1424
[12] Goodenough J B, Wold A, Arnott R J and Menyuk N 1961 *Phys. Rev.* **124** 373
[13] Blasse G 1965 *J. Phys. Chem. Solids* **26** 1969
[14] Troyanchuk I O, Lobanovsky L S, Khalyavin D D, Pastushonok S N and Szymczak H 2000 *J. Magn. Magn. Mater.* **210** 63
[15] Joy P A, Khollam Y B, Patole S N and Date S K 2000 *Mater. Lett.* **46** 261
[16] Autret C, Hejtmanek J, Knizek K, Marysko M, Jirak Z, Dlouha M and Vratislav S 2005 *J. Phys.: Condens. Matter* **17** 1601
[17] Maignan A, Damay F, Barnabe A, Martin C, Hervieu M and Raveau B 1998 *Phil. Trans. R. Soc.* A **356** 1635
[18] Park J-H, Cheong S-W and Chen C T 1997 *Phys. Rev.* B **55** 11072
[19] Van Elp J 1999 *Phys. Rev.* B **60** 7649
[20] Joy P A, Khollam Y B and Date S K 2000 *Phys. Rev.* B **62** 8608
[21] Koningsberger D C and Prins R (ed) 1988 *Principles, Applications, Techniques EXAFS, SEXAFS and XANES* (New York: Wiley)
[22] Sikora M, Kapusta Cz, Jirak Z, Autret C, Borowiec M, Oates C J, Prochazka V, Rybicki D and Zajac D 2006 *Phys. Rev.* B **73** 094426
[23] Prochazka V, Kapusta Cz, Sikora M, Zajac D, Knizek Z K, Jirak Z and Stepankova H 2007 *J. Magn. Magn. Mater.* **310** E197
[24] Rodriguez-Carvajal J 1990 *Abstracts of the Satellite Mtg on Powder Diffraction of the XV Congr. of IUCR* p 127
[25] Karus W and Nolze G 1996 *J. Appl. Crystallogr.* **29** 301
[26] Newville M 2001 *J. Synchrotron Radiat.* **8** 322
[27] Zabinsky S I, Rehr J J, Ankudinov A, Albers R C and Eller M J 1995 *Phys. Rev.* B **52** 2995
[28] Ravel B 2001 *J. Synchrotron Radiat.* **8** 314
[29] Stern E A, Newville M, Ravel B, Yacoby Y and Haskel D 1995 *Physica* B **208/209** 117
[30] Shibata T, Bunker B A and Mitchell J F 2003 *Phys. Rev.* B **68** 024103
[31] Subias G, Garcia J, Blasco J and Proieti M G 1998 *Phys. Rev.* B **57** 748
[32] Subias G, Garcia J, Proieti M G and Blasco J 1997 *Phys. Rev.* B **56** 8183
[33] Booth C H, Bridges F, Kwei G H, Lawrence J M, Cornelius A L and Neumeier J J 1998 *Phys. Rev.* B **57** 10440
[34] Meneghini C, Castellano C, Mobilio S, Kumar A, Ray S and Sarma D D 2002 *J. Phys.: Condens. Matter* **14** 1967
[35] Dass R I and Goodenough J B 2003 *Phys. Rev.* B **67** 014401
[36] Bull C L, Gleeson D and Knight K S 2003 *J. Phys.: Condens. Matter* **15** 4927
[37] Radaelli P G, Iannone G, Marezio M, Hwang H Y, Cheong S-W, Jorgenson J D and Argyriou D N 1997 *Phys. Rev.* B **56** 8265
[38] Medarde M, Mesot J, Lacorre P, Rosenkranz S, Fischer P and Gobrecht K 1995 *Phys. Rev.* B **52** 9248